Published in final edited form as:
J Neurol Neurosurg Psychiatry. 2009 June ; 80(6): 659–666. doi:10.1136/jnnp.2007.126219.

Deep brain stimulation activation volumes and their association with neurophysiological mapping and therapeutic outcomes

Christopher B. Maks[1], **Christopher R. Butson**[1], **Benjamin L. Walter**[2], **Jerrold L. Vitek**[2,3], and **Cameron C. McIntyre**[1,2,*]

[1]Department of Biomedical Engineering, Cleveland Clinic Foundation, Cleveland, OH

[2]Center for Neurological Restoration, Cleveland Clinic Foundation, Cleveland, OH

[3]Department of Neurosciences, Cleveland Clinic Foundation, Cleveland, OH

Abstract

Objective—Despite the clinical success of deep brain stimulation (DBS) for the treatment of Parkinson's disease (PD), little is known about the electrical spread of the stimulation. The primary goal of this study was to integrate neuroimaging, neurophysiology, and neurostimulation data sets from 10 PD patients, unilaterally implanted with subthalamic nucleus (STN) DBS electrodes, to identify the theoretical volume of tissue activated (VTA) by clinically defined therapeutic stimulation parameters.

Methods—Each patient-specific model was created with a series of five steps: 1) definition of the neurosurgical stereotactic coordinate system within the context of pre-operative imaging data; 2) entry of intra-operative microelectrode recording locations from neurophysiologically defined thalamic, subthalamic, and substantia nigra neurons into the context of the imaging data; 3) fitting a 3D brain atlas to the neuroanatomy and neurophysiology of the patient; 4) positioning the DBS electrode in the documented stereotactic location, verified by post-operative imaging data; and 5) calculation of the VTA using a diffusion tensor based finite element neurostimulation model.

Results—The patient-specific models show that therapeutic benefit was achieved with direct stimulation of a wide range of anatomical structures in the subthalamic region. Interestingly, of the 5 patients exhibiting a greater than 40% improvement in their unified PD rating scale (UPDRS), all but one had the majority of their VTA outside the atlas defined borders of the STN. Further, of the 5 patients with less than 40% UPDRS improvement all but one had the majority of their VTA inside the STN.

Conclusions—Our results are consistent with previous studies suggesting that therapeutic benefit is associated with electrode contacts near the dorsal border of the STN, and provide quantitative estimates of the electrical spread of the stimulation in a clinically relevant context.

*Corresponding Author: Cameron C. McIntyre, Ph.D., Department of Biomedical Engineering, Cleveland Clinic Foundation, 9500 Euclid Ave. ND20, Cleveland, OH 44195, mcintyc@ccf.org, PHONE: (216) 445-3264, FAX: (216) 444-9198.

Conflict of Interest Statement: CBM, CRB and CCM authored intellectual property related to the project methodology. CRB and CCM hold company shares in IntElect Medical Inc.

Keywords

Parkinson's disease; subthalamic nucleus; stereotactic neurosurgery; surgical planning; microelectrode recording

INTRODUCTION

Deep brain stimulation (DBS) of the subthalamic nucleus (STN), and its surrounding anatomical structures, is an effective treatment for the motor symptoms associated with advanced Parkinson's disease (PD) [1;2;3;4]. Despite the clinical success of DBS, debate continues on its therapeutic mechanisms of action, and little is known about the electrical spread of DBS in the context of clinical outcomes. Previous studies have examined relationships between the stimulation parameter settings and the therapeutic response to DBS [5;6;7;8;9;10]. In addition, extensive effort has been dedicated to identifying the anatomical location of therapeutic electrode contacts in the STN region [11;12;13;14;[15,16,17,18,19];20;21;22;23]. However, only recently have methodological tools been developed that can link the scientific analysis of both anatomical and electrical models of human DBS [24;25;26;27]. In this study we integrated neuroimaging, neurophysiology, and neurostimulation data sets to define the therapeutic volume of tissue activated (VTA) by DBS electrodes unilaterally implanted in the STN region of 10 PD patients.

The STN is a relatively small structure surrounded by a number of different fiber pathways and gray matter areas. When DBS is applied to the STN region, it remains unclear which neural response(s) from the surrounding anatomical structure(s) are directly responsible for the therapeutic or non-therapeutic effects of stimulation. Converging theoretical [28] and experimental [29] results suggest that therapeutic DBS in the STN region generates an excitatory effect on axons surrounding the electrode. While correlations between axonal activation and the therapeutic mechanisms of DBS remain controversial, one possible hypothesis is that high frequency stimulation overrides the underlying pathological neural activity patterns [30;31;32;33]. Therefore, the approach taken in this study was to quantify the volume of axonal tissue directly stimulated by clinically defined therapeutic stimulation parameters. We hypothesized that direct axonal activation from therapeutic DBS would spread outside the anatomical borders of the STN [24]. Previously we developed and validated a methodology to predict and visualize the VTA during DBS on a patient-specific basis [26]. Here we apply those methods to identify relationships between the VTA, its overlap with a 3D anatomical model of the STN, and the degree of therapeutic benefit achieved by the stimulation.

METHODS

Patient Population

Following the methodology described in Butson et al. [26] we developed 10 patient-specific models of DBS in the STN region. Subject selection was performed retrospectively from a database of DBS patients implanted at the Cleveland Clinic. Patients were identified that fulfilled four important criteria. First, each patient had idiopathic PD as defined by the UK Brain Bank Criteria [34], and demonstrated >40% improvement in their Unified Parksinson's Disease Rating Score (UPDRS) motor examination (part III) to dopamine replacement therapy, suggesting that they would respond well to DBS therapy. Second, each patient achieved their clinically defined maximum therapeutic benefit via monopolar cathodic stimulation, thereby simplifying the theoretical calculations of the neural response to DBS. Third, each patient was unilaterally implanted, ensuring that the measured DBS effects were the direct result of the single stimulation site. Fourth, patients exhibited a wide

range of therapeutic benefit from DBS, allowing for comparison between good and bad responders. The 10 patients were identified and the clinical/imaging data was assembled prior to the development of the patient-specific computer models (Table 1). In turn, we had no *a priori* knowledge of relationships between the anatomical location of the electrode, the volume of tissue activated (VTA), or the therapeutic outcomes in the selected patients. This study was approved by the Cleveland Clinic Institutional Review Board.

Prior to surgery, each patient was evaluated with the UPDRS [35] in both the off medication and on medication states. Subsequently, each patient underwent a unilateral, microelectrode guided, stereotactic neurosurgical procedure to implant the DBS electrode into the STN region [36]. Several months after the surgery, once standard clinical care had defined a stable therapeutic stimulation parameter setting (Table 1), each patient was again evaluated with the UPDRS under two conditions: off medication / off stimulation (OFF MEDS / OFF STIM); and off medication / on stimulation (OFF MEDS / ON STIM).

Imaging and Co-Registration

Each patient underwent pre-operative computed tomography (CT) and/or magnetic resonance imaging (MRI) as part of the standard DBS surgical protocol. The CT/MRI data documented the orientation of the patient's anatomy relative to their stereotactic neurosurgical frame (Leksell model G (Elekta Corp., Stockholm, Sweden)) (Fig. 1). The coordinate system associated with the stereotactic frame (frame-space) was defined in our model system using fiducial markers in the imaging data (Fig 1A). The patient-specific DBS model, and all imaging data, used frame-space as the unifying coordinate system. Therefore, in instances where the pre-operative MRI did not include the frame fiducials, the MRI was co-registered with the pre-operative CT that did have the frame fiducials. Each patient also underwent a post-operative CT to verify the DBS lead location in the brain, and this image was also co-registered to the frame-space image.

Each image co-registration was performed using Analyze 7.0 (AnalyzeDirect, Lenexa, KS, USA). We used the ITK 3D-registration function in Analyze, followed by manual adjustment to precisely match the positions of the anterior and posterior commissures. Co-registrations involving two or more data sets from the same patient required only rotation and translation to yield near-perfect overlaps.

The fundamental basis of location in our model system was strict adherence to the stereotactic coordinate system established by the neurosurgical frame. The major advantage of using frame-space in our model system was the ability to precisely place microelectrode recording (MER) data in the context of the MRI (see below). MER data was acquired with a microelectrode placed within a microdrive unit that was attached to the frame with a specific trajectory (arc angle, ring angle, and target point) defined in the stereotactic coordinate system. In turn, as the microelectrode advanced into the brain, its location could be defined as a specific point in the stereotactic coordinate system (and the patient brain as viewed in the MRI).

The anatomical images of each patient were also co-registered with a diffusion tensor MRI (DTI) atlas brain [37]. The DTI atlas brain represented the basis for the DBS electric field model (see below). Rotation, translation and, in some cases, scaling were all necessary to perform this co-registration. To account for pitch and yaw differences in the images, the intra-commissural line (ICL) of the DTI atlas brain was aligned to the ICL of the patient. The DTI atlas brain was then scaled along the anterior-posterior axis to bring the anterior commissure (AC) and posterior commissure (PC) into coincidence with the patient MRI counterparts. Next, the DTI atlas brain was scaled along the dorsal-ventral and medial-lateral axes and rotated about the anterior-posterior axis, as needed. This final rotation

ensured the DTI atlas brain featured the same degree of roll found in the patient's image. The transformation matrix representing the net alteration performed on the DTI atlas brain to align it with a patient's frame-space image was:

[Atlas].

This matrix governed the transition from DTI atlas-space to a patient's frame-space and its inverse describes the opposite. Two additional transformation matrices were also generated:

[Frame]

describing the exact position of the stereotactic frame relative to the co-registered imaging data and:

[Origin]

a purely translational matrix cataloguing the shift from the origin of the co-registered imaging data to the origin of frame-space.

MER Data and DBS Lead Placement

Prior to permanent surgical implantation of the DBS electrode in the patient, MER of neuronal activity was performed in the operating room (OR) to further characterize the stereotactic location of the STN [38;39] (Fig. 1B–D). The patients analyzed in this study had 3 to 6 MER trajectories each (a.k.a. tracks) (Table 2). The MER data were added into a patient's model by applying their frame-space transformation matrix, *[Frame]*, to an indicated trajectory and depth as documented in the OR notes. An additional matrix representing a given trajectory relative to the co-registered imaging data was required as a precursor:

[Trajectory].

This process allowed for each MER data point (electrophysiologically identified cell type and stereotactic location) to be visualized within the imaging data and 3D brain atlas (see below) representations for the given patient (Fig. 1B–D).

The intended stereotactic surgical placement of the DBS electrode was added into a patient's model in the same fashion (Fig. 1E). The modeled DBS lead locations were verified by viewing the patient's co-registered post-operative image concurrently with their modeled DBS lead location. The radiological artifact from the implanted electrode outlined the model electrode in each patient of this study.

3D Brain Atlas Nuclei

Once a patient's model was populated with their MER data, 3D atlas representations of the thalamus, globus pallidus, caudate, and STN were added to the model system (Fig. 1C,D). The 3D atlas nuclei were originally customized to the neuroanatomy of the DTI atlas brain [26]. Therefore, the 3D atlas nuclei were scaled and translated to fit each patient. The goal was to use the anatomical information provided in the pre-operative MRI with the neurophysiological information provided by the MER tracks to achieve the best possible fit (Fig. 1; Table 2). The initial placement of the 3D atlas nuclei into the patient brain was

governed by the matrix describing the DTI atlas - to - patient MRI co-registration, *[Atlas]*. Next, the nuclei were translated such that their boundaries best encapsulated their respective cell-types as detected by MER. Translations were applied uniformly to all nuclei so that their positioning relative to one another was preserved. Once an acceptable fit was established based on the MER data, the patients MRI was taken into consideration. Anatomy visible in the MRI (thalamus, pallidum, caudate) served as a guide to further converge the positioning of the 3D nuclei to the best possible manual fit. In situations where both MER and MRI data could not be maximally accommodated, MER took precedence. This decision was justified because the overriding goal was to orient atlas surfaces as accurately as possible with respect to the patient's DBS electrode, and the relative position of the MER data was the basis for the surgical DBS electrode placement. The net translational adjustment that brought the atlas nuclei in line with the patient data was recorded as:

$$[\text{Nuclei}].$$

Table 2 shows the percentage of STN MER points that were contained within the atlas defined borders of each patient's fitted STN.

VTA Generation

The Butson et al. [26] human DBS modeling system was designed to provide anatomically and electrically accurate predictions of the VTA as a function of the stimulation parameter settings (Figure 1F). Each patient-specific DBS model included explicit representation of four important factors in calculating the neural response to DBS: 1) accurate reconstruction of the stimulus waveform generated by the implanted pulse generator [40], 2) capacitance of the electrode-tissue interface which modulates the shape of the stimulus waveform transmitted into the tissue medium [41], 3) high resistance sheath of encapsulation tissue surrounding the DBS electrode to appropriately account for the impedance of the electrode-tissue interface [42], and 4) diffusion tensor based 3D anisotropic and inhomogeneous tissue electrical properties that surround DBS electrodes [26]. We converted the Wakana et al. [37] diffusion tensor MRI atlas brain into a set of conductivity tensors as proposed by Tuch et al. [43]. These conductivity tensors were then mapped into the 3D finite element mesh, allowing for solution of the time and space dependent potential distribution generated by a DBS electrode implanted in the STN [26].

A transformation matrix was calculated to define each patient's DBS electrode location in the context of the DTI brain atlas-space:

$$[\text{DTI}]=[\text{Atlas}]^{-1} \times [\text{Origin}]^{-1} \times [\text{Nuclei}]^{-1} \times [\text{Frame}] \times [\text{Trajectory}].$$

A model solution of the voltage distribution in the brain was generated for the patient's therapeutic stimulation parameters (contact, impedance, amplitude, frequency, pulse width), and a VTA was calculated based on the second spatial derivative of the voltage [26] (Fig. 1F). The VTA can be interpreted as a region where the axons that pass through the volume will generate propagating action potentials at the stimulation frequency. The DBS model simulations were performed on an 8 processor SGI Prism (Silicon Graphics Inc., Mountain View, CA) with 36 GB of shared memory using BioPSE (Scientific Computing & Imaging Institute, University of Utah).

RESULTS

The 10 PD patients analyzed in this study exhibited a wide range of therapeutic benefit from unilateral DBS of the subthalamic region (Table 3). The best responders exhibited UPDRS improvements from DBS that were near to or better than their UPDRS improvements from medication alone. Conversely, the worst responders exhibited UPDRS improvements from DBS that were less than their response to medication alone. Patients were selected with a range of therapeutic outcomes to provide an opportunity to identify commonalities among patients with expected and less than expected improvement from DBS. The patients were ordered from 1 to 10 with patient 1 having the greatest improvement from DBS and patient 10 having the least improvement. This designation was defined by the percentage improvement in their post-operative OFF MEDS UPDRS motor evaluations in the OFF DBS and ON DBS conditions.

The VTA generated by each patient's clinically defined therapeutic stimulation parameter settings was calculated and its overlap with the surrounding neuroanatomy was defined (Figure 2, Table 3). Our theoretical calculations predicted an average stimulation volume of 71 mm^3, and each VTA was smaller than the ~200 mm^3 total volume of the 3D STN model (exact volume depended on the 3D brain atlas fitting). Every patient had at least some of their VTA intersect with the STN; however, every patient also had some of their VTA spread outside the borders of the STN. Interesting differences between the overlap of the VTA and STN arose when we compared the five best outcomes (patients 1–5) to the five worst outcomes (patients 6–10) (Figure 2, Table 3). Patients 1–5 all exhibited a greater than 40% UPDRS improvement with unilateral DBS. Of these five patients, four had more than half of their VTA outside of the STN. Patients 6–10 all exhibited a less than 40% UPDRS improvement with unilateral DBS and four of the five had more than half of their VTA inside of the STN.

The integration of multiple data sets (imaging, MER, atlas, VTA) in our study carried with it numerous registrations where the accuracy was limited by imaging resolution. Therefore, to address the impact of uncertainty in the DBS electrode location relative to the underlying neuroanatomy we preformed a sensitivity analysis on the overlap of the VTA and STN with a range of DBS electrode locations in each patient. The DBS electrode was moved by 1 mm in the anterior, posterior, dorsal, ventral, medial, or lateral directions relative to its originally defined stereotactic implant location, and a new VTA was calculated for each new electrode location (Figure 3; Table 4). These perturbations did not substantially change the calculated volume of stimulated tissue in each patient, nor did they alter the result that 4 out of the 5 best responders had the majority of their VTA outside of the STN, and 4 out of the 5 worst responders had the majority of their VTA inside the STN.

DISCUSSION

The goal of this study was to integrate detailed computer modeling with clinical outcomes analysis to enhance understanding of the effects of DBS of the subthalamic region. We developed 10 patient-specific models of unilateral DBS based on neuroimaging, neurophysiology, neuroanatomy, and neurostimulation data. Our results suggest that direct stimulation of the STN is only one of multiple neuroanatomical territories in the STN region that may play a role in the therapeutic benefit achieved with DBS.

Our theoretical models show that direct activation of ~70 mm^3 of axonal tissue dorsal, lateral, and posterior to the geometric center (or centroid) of the atlas defined STN generated therapeutic benefit from DBS (Figure 3). This general area includes the sensorimotor territory of the STN that is believed to be involved in motor control, and whose

physiological activity is altered in Parkinson's disease [38]. Patients with the best clinical outcomes also tended to have a higher percentage of direct stimulation of axonal tissue outside of, and dorsal to, the STN. Similar conclusions have been reached by several previous investigations examining the anatomical location of therapeutic electrode contacts [e.g. 16;20], while others have suggested that optimal DBS contacts were located in the dorsolateral sensorimotor STN, but not the white matter dorsal to the STN [e.g. 17].

Debate on the "optimal" implantation location for DBS electrodes will undoubtedly continue over the next decade as new techniques enable more detailed analysis of the anatomical, electrical, and behavioral variables of DBS. The evolutionary addition of this study to the previous literature is the quantitative integration of clinical outcomes analysis and electrically accurate models of the spread of stimulation [24;26]. This process allowed us to critically examine the interaction between the volumes of tissue activated (VTA) and the underlying neurophysiology and neuroanatomy.

Given that the fundamental purpose of DBS is to modulate neural activity with electric fields, it is imperative that scientific analyses of DBS attempt to account for the variables associated with clinical stimulation parameter selection (contact, impedance, voltage, pulse width, frequency) and the resulting spread of stimulation relative to the anatomy. Our patient-specific DBS modeling system uses some of the most advanced neurostimulation prediction techniques currently available. However, it should be noted that there are several limitations in this study. First, we selected patients with monopolar stimulation to simplify calculations of the neural response to DBS. This selection criterion may have biased our analysis away from patients with lateral electrodes who have capsular spread limiting benefit, as these patients are typically reprogrammed to bipolar stimulation. Second, the co-registration of multiple images and atlas representations of the patient creates spatial variability that can not be ignored. We attempted to minimize co-registration error by using easily identifiable landmarks such as the AC / PC and widely accepted co-registration algorithms. Third, while we extended great effort to place all of our data into the stereotactic coordinate system of the patient to utilize MER data in the most accurate way possible, one caveat was the inherent uncertainty in the intra-operative electro-physiologist's anatomical designation of the recordings. However, we used established criteria (e.g. increased background activity followed by the presence of neuronal activity with discharge patterns similar to that previously described by the STN, along with the presence of sensorimotor responses) to make the MER designations used in our study [38]. Fourth, outside of histological reconstruction it is impossible to know the exact size, shape, and location of the STN in a given patient [44;45;46]. We relied on a 3D atlas model fit to match boundaries defined by the recorded neurophysiology and neuroanatomy visible on the MRI. Fifth, due to signal-to-noise considerations, the DTI brain atlas used in this study was acquired with relatively large voxel sizes [37]; therefore, the 3D tissue conductivities used in the model only represent a gross estimate. Sixth, the VTA prediction functions used in the model were derived from the activation of straight, relatively large diameter myelinated axons, and may not be representative of the response of other neuron types surrounding the electrode (local projection neurons, local interneurons, afferent inputs, etc.). Given that myelinated axons are considered the most excitable neuron type to extracellular electrical stimulation [47]; our VTA predictions should be considered an upper limit in terms of stimulation spread.

Experimental validation of the VTA predictions is a difficult task. We are actively pursuing research studies that link our DBS models with electrophysiological recordings in humans and non-human primates [26;28;48]. The results of these studies show that our models can accurately predict stimulation spread into the corticospinal tract during STN DBS, and the synergistic evolution of our modeling technology and experimental analysis will allow for continuous improvement in their accuracy and validity. Nonetheless, we believe that the

patient-specific DBS modeling system used in this study is capable of making quantitative, clinically relevant, predictions.

Our results suggest that stimulation of axonal tissue dorsal, lateral, and posterior to the centroid of the STN maximizes therapeutic benefit from DBS. However, every patient's disease pathology, electrode location, and behavioral response to stimulation are different. For example, patients 2, 7, and 9 all had therapeutic VTAs with similar sizes and anatomical locations, but their therapeutic outcomes showed substantial differences. In turn, maximizing therapeutic benefit for an individual DBS patient involves more than just electrode placement and a VTA calculation, as many variables unaccounted for in this study could impact the behavioral response to DBS. For example, it is possible that based on the patient's symptoms one electrode location may be preferential to another, or stimulation spread into one anatomical region may be preferential to another. In turn, the interplay between the patient and clinician performing the DBS parameter selection is critical in defining the balance between therapeutic benefit and side effects. However, this clinical process is typically done without the opportunity to visualize the regional spread of stimulation and its location with respect to the surrounding anatomy. This could be an important issue in patients like 6 and 8 where the model suggests that the electrodes are in a good location, but the stimulation parameter settings may not be optimal because of stimulation spread into the internal capsule. And the converse is suggested with patient 10 where a lateral electrode location limits the allowable size of the VTA to avoid spread into internal capsule. Therefore, the next step along this line of research is to couple patient-specific DBS model predictions with prospective clinical evaluations to develop new and improved techniques to optimize the clinical efficacy of DBS. For example, methodology from this study may find utility in augmenting DBS surgical placement planning [46;49;50;51], and the post-operative stimulation parameter selection process [52].

Acknowledgments

This work was supported by grants from the Ohio Biomedical Research and Technology Transfer Partnership, Wallace H. Coulter Foundation, and National Institutes of Health (NS050449, NS052042 & NS059736). The authors would also like to thank Susumu Mori for providing the diffusion tensor image brain atlas data set, Jaimie Henderson for providing the 3D brain atlas volumes, Barbara Wolgamuth for assistance with the clinical data collection, and Scott Cooper for helpful discussion on this project.

REFERENCES

1. Limousin P, Krack P, Pollak P, Benazzouz A, Ardouin C, Hoffmann D, Benabid AL. Electrical stimulation of the subthalamic nucleus in advanced Parkinson's disease. N Engl J Med 1998;339(16):1105–1111. [PubMed: 9770557]
2. Obeso JA, Olanow CW, Rodriguez-Oroz MC, Krack P, Kumar R, Lang AE. Deep-brain stimulation of the subthalamic nucleus or the pars interna of the globus pallidus in Parkinson's disease. N Engl J Med 2001;345(13):956–963. [PubMed: 11575287]
3. Krack P, Batir A, Van Blercom N, Chabardes S, Fraix V, Ardouin C, Koudsie A, Limousin PD, Benazzouz A, LeBas JF, Benabid AL, Pollak P. Five-year follow-up of bilateral stimulation of the subthalamic nucleus in advanced Parkinson's disease. N Engl J Med 2003;349(20):1925–1934. [PubMed: 14614167]
4. Rodriguez-Oroz MC, Obeso JA, Lang AE, Houeto JL, Pollak P, Rehncrona S, Kulisevsky J, Albanese A, Volkmann J, Hariz MI, Quinn NP, Speelman JD, Guridi J, Zamarbide I, Gironell A, Molet J, Pascual-Sedano B, Pidoux B, Bonnet AM, Agid Y, Xie J, Benabid AL, Lozano AM, Saint-Cyr J, Romito L, Contarino MF, Scerrati M, Fraix V, Van Blercom N. Bilateral deep brain stimulation in Parkinson's disease: a multicentre study with 4 years follow-up. Brain 2005;128(10): 2240–2249. [PubMed: 15975946]

5. Benabid AL, Pollak P, Gao D, Hoffmann D, Limousin P, Gay E, Payen I, Benazzouz A. Chronic electrical stimulation of the ventralis intermedius nucleus of the thalamus as a treatment of movement disorders. J Neurosurg 1996;84(2):203–214. [PubMed: 8592222]
6. Rizzone M, Lanotte M, Bergamasco B, Tavella A, Torre E, Faccani G, Melcarne A, Lopiano L. Deep brain stimulation of the subthalamic nucleus in Parkinson's disease: effects of variation in stimulation parameters. J Neurol Neurosurg Psychiatry 2001;71(2):215–219. [PubMed: 11459896]
7. Moro E, Esselink RJ, Xie J, Hommel M, Benabid AL, Pollak P. The impact on Parkinson's disease of electrical parameter settings in STN stimulation. Neurology 2002;59(5):706–713. [PubMed: 12221161]
8. O'Suilleabhain PE, Frawley W, Giller C, Dewey RB. Tremor response to polarity, voltage, pulsewidth and frequency of thalamic stimulation. Neurology 2003;60(5):786–790. [PubMed: 12629234]
9. Timmermann L, Wojtecki L, Gross J, Lehrke R, Voges J, Maarouf M, Treuer H, Sturm V, Schnitzler A. Ten-hertz stimulation of subthalamic nucleus deteriorates motor symptoms in Parkinson's disease. Mov Disord 2004;19(11):1328–1333. [PubMed: 15389990]
10. Kuncel AM, Cooper SE, Wolgamuth BR, Clyde MA, Snyder SA, Montgomery EB Jr, Rezai AR, Grill WM. Clinical response to varying the stimulus parameters in deep brain stimulation for essential tremor. Mov Disord 2006;21(11):1920–1928. [PubMed: 16972236]
11. Lanotte MM, Rizzone M, Bergamasco B, Faccani G, Melcarne A, Lopiano L. Deep brain stimulation of the subthalamic nucleus: anatomical, neurophysiological, and outcome correlations with the effects of stimulation. J Neurol Neurosurg Psychiatry 2002;72(1):53–58. [PubMed: 11784826]
12. Saint-Cyr JA, Hoque T, Pereira LC, Dostrovsky JO, Hutchison WD, Mikulis DJ, Abosch A, Sime E, Lang AE, Lozano AM. Localization of clinically effective stimulating electrodes in the human subthalamic nucleus on magnetic resonance imaging. J Neurosurg 2002;97(5):1152–1166. [PubMed: 12450038]
13. Starr PA, Christine CW, Theodosopoulos PV, Lindsey N, Byrd D, Mosley A, Marks WJ Jr. Implantation of deep brain stimulators into the subthalamic nucleus: technical approach and magnetic resonance imaging-verified lead locations. J Neurosurg 2002;97(2):370–387. [PubMed: 12186466]
14. Voges J, Volkmann J, Allert N, Lehrke R, Koulousakis A, Freund HJ, Sturm V. Bilateral high-frequency stimulation in the subthalamic nucleus for the treatment of Parkinson disease: correlation of therapeutic effect with anatomical electrode position. J Neurosurg 2002;96(2):269–279. [PubMed: 11838801]
15. Hamel W, Fietzek U, Morsnowski A, Schrader B, Herzog J, Weinert D, Pfister G, Muller D, Volkmann J, Deuschl G, Mehdorn HM. Deep brain stimulation of the subthalamic nucleus in Parkinson's disease: evaluation of active electrode contacts. J Neurol Neurosurg Psychiatry 2003;74(8):1036–1046. [PubMed: 12876231]
16. Yelnik J, Damier P, Demeret S, Gervais D, Bardinet E, Bejjani BP, Francois C, Houeto JL, Arnule I, Dormont D, Galanaud D, Pidoux B, Cornu P, Agid Y. Localization of stimulating electrodes in patients with Parkinson disease by using a three-dimensional atlas-magnetic resonance imaging coregistration method. J Neurosurg 2003;99(1):89–99. [PubMed: 12854749]
17. Herzog J, Fietzek U, Hamel W, Morsnowski A, Steigerwald F, Schrader B, Weinert D, Pfister G, Muller D, Mehdorn HM, Deuschl G, Volkmann J. Most effective stimulation site in subthalamic deep brain stimulation for Parkinson's disease. Mov Disord 2004;19(9):1050–1054. [PubMed: 15372594]
18. Zonenshayn M, Sterio D, Kelly PJ, Rezai AR, Beric A. Location of the active contact within the subthalamic nucleus (STN) in the treatment of idiopathic Parkinson's disease. Surg Neurol 2004;62(3):216–225. [PubMed: 15336862]
19. Nowinski WL, Belov D, Pollak P, Benabid AL. Statistical analysis of 168 bilateral subthalamic nucleus implantations by means of the probabilistic functional atlas. Neurosurgery 2005;57:319–330. [PubMed: 16234681]
20. Plaha P, Ben-Shlomo Y, Patel NK, Gill SS. Stimulation of the caudal zona incerta is superior to stimulation of the subthalamic nucleus in improving contralateral parkinsonism. Brain 2006;129(7):1732–1747. [PubMed: 16720681]

21. Godinho F, Thobois S, Magnin M, Guenot M, Polo G, Benatru I, Xie J, Salvetti A, Garcia-Larrea L, Broussolle E, Mertens P. Subthalamic nucleus stimulation in Parkinson's disease : anatomical and electrophysiological localization of active contacts. J Neurol 2006;253(10):1347–1355. [PubMed: 16788774]
22. Yokoyama T, Ando N, Sugiyama K, Akamine S, Namba H. Relationship of stimulation site location within the subthalamic nucleus region to clinical effects on parkinsonian symptoms. Stereotact Funct Neurosurg 2006;84(4):170–175. [PubMed: 16905883]
23. Guehl D, Edwards R, Cuny E, Burbaud P, Rougier A, Modolo J, Beuter A. Statistical determination of the optimal subthalamic nucleus stimulation site in patients with Parkinson disease. J Neurosurg 2007;106(1):101–110. [PubMed: 17236495]
24. McIntyre CC, Mori S, Sherman DL, Thakor NV, Vitek JL. Electric field and stimulating influence generated by deep brain stimulation of the subthalamic nucleus. Clin Neurophysiol 2004;115(3): 589–595. [PubMed: 15036055]
25. Hemm S, Mennessier G, Vayssiere N, Cif L, El Fertit H, Coubes P. Deep brain stimulation in movement disorders: stereotactic coregistration of two-dimensional electrical field modeling and magnetic resonance imaging. J Neurosurg 2005;103(6):949–955. [PubMed: 16381180]
26. Butson CR, Cooper SC, Henderson JM, McIntyre CC. Patient-specific analysis of the volume of tissue activated during deep brain stimulation. NeuroImage 2007;34(2):661–670. [PubMed: 17113789]
27. Sotiropoulos SN, Steinmetz PN. Assessing the direct effects of deep brain stimulation using embedded axon models. J Neural Eng 2007;4(2):107–119. [PubMed: 17409485]
28. Miocinovic S, Parent M, Butson CR, Hahn PJ, Russo GS, Vitek JL, McIntyre CC. Computational analysis of subthalamic nucleus and lenticular fasciculus activation during therapeutic deep brain stimulation. J Neurophysiol 2006;96(3):1569–1580. [PubMed: 16738214]
29. Hashimoto T, Elder CM, Okun MS, Patrick SK, Vitek JL. Stimulation of the subthalamic nucleus changes the firing pattern of pallidal neurons. J Neurosci 2003;23(5):1916–1923. [PubMed: 12629196]
30. Montgomery EB, Baker KB. Mechanisms of deep brain stimulation and future technical developments. Neurol Res 2000;22(3):259–266. [PubMed: 10769818]
31. Vitek JL. Mechanisms of deep brain stimulation: excitation or inhibition. Mov Disord 2002;17:S69–S72. [PubMed: 11948757]
32. Grill WM, Snyder AN, Miocinovic S. Deep brain stimulation creates an informational lesion of the stimulated nucleus. Neuroreport 2004;15(7):1137–1140. [PubMed: 15129161]
33. McIntyre CC, Savasta M, Walter BL, Vitek JL. How does deep brain stimulation work? Present understanding and future questions. J Clin Neurophysiol 2004;21(1):40–50. [PubMed: 15097293]
34. Hughes AJ, Daniel SE, Kilford L, Lees AJ. Accuracy of clinical diagnosis of idiopathic Parkinson's disease: a clinico-pathological study of 100 cases. J Neurol Neurosurg Psychiatry 1992;55(3):181–184. [PubMed: 1564476]
35. Fahn, S.; Elton, RL. Members of the UPDRS Development Committee. The Unified Parkinson's Disease Rating Scale. In: Fahn, S.; Marsden, CD.; Calne, DB., editors. Recent developments in Parkinson's Disease. Vol. 2. Florham Park, NJ: McMillan Healthcare Information; 1987. p. 293-304.
36. Machado A, Rezai AR, Kopell BH, Gross RE, Sharan AD, Benabid AL. Deep brain stimulation for Parkinson's disease: surgical technique and perioperative management. Mov Disord 2006:S247–S258. [PubMed: 16810722]
37. Wakana S, Jiang H, Nagae-Poetscher LM, van Zijl PC, Mori S. Fiber tract-based atlas of human white matter anatomy. Radiology 2004;230(1):77–87. [PubMed: 14645885]
38. Rodriguez-Oroz MC, Rodriguez M, Guridi J, Mewes K, Chockkman V, Vitek J, DeLong MR, Obeso JA. The subthalamic nucleus in Parkinson's disease: somatotopic organization and physiological characteristics. Brain 2001;124(9):1777–1790. [PubMed: 11522580]
39. Walter BL, Vitek JL. Surgical treatment for Parkinson's disease. Lancet Neurol 2004;3(12):719–728. [PubMed: 15556804]

40. Butson CR, McIntyre CC. Differences among implanted pulse generator waveforms cause variations in the neural response to deep brain stimulation. Clin Neurophysiol 2007;118(8):1889–1894. [PubMed: 17581776]
41. Butson CR, McIntyre CC. Tissue and electrode capacitance reduce neural activation volumes during deep brain stimulation. Clin Neurophysiol 2005;116(10):2490–2500. [PubMed: 16125463]
42. Butson CR, Maks CB, McIntyre CC. Sources and effects of electrode impedance during deep brain stimulation. Clin Neurophysiol 2006;117(2):447–454. [PubMed: 16376143]
43. Tuch DS, Wedeen VJ, Dale AM, George JS, Belliveau JW. Conductivity tensor mapping of the human brain using diffusion tensor MRI. Proc Natl Acad Sci U S A 2001;98(20):11697–11701. [PubMed: 11573005]
44. Hardman CD, Henderson JM, Finkelstein DI, Horne MK, Paxinos G, Halliday GM. Comparison of the basal ganglia in rats, marmosets, macaques, baboons, and humans: volume and neuronal number for the output, internal relay, and striatal modulating nuclei. J Comp Neurol 2002;445(3):238–255. [PubMed: 11920704]
45. Nowinski WL, Liu J, Thirunavuukarasuu A. Quantification and visualization of the three-dimensional inconsistency of the subthalamic nucleus in the Schaltenbrand-Wahren brain atlas. Stereotact Funct Neurosurg 2006;84(1):46–55. [PubMed: 16741377]
46. Yelnik J, Bardinet E, Dormont D, Malandain G, Ourselin S, Tande D, Karachi C, Ayache N, Cornu P, Agid Y. A three-dimensional, histological and deformable atlas of the human basal ganglia. I. Atlas construction based on immunohistochemical and MRI data. Neuroimage 2007;34(2):618–638. [PubMed: 17110133]
47. Ranck JB. Which elements are excited in electrical stimulation of mammalian central nervous system: a review. Brain Res 1975;98(3):417–440. [PubMed: 1102064]
48. Chaturvedi, A.; Butson, CR.; Cooper, SE.; McIntyre, CC. Subthalamic nucleus deep brain stimulation: accurate axonal threshold prediction with diffusion tensor based electric field models. 28th Int. Conf. IEEE-EMBS; New York, NY; 2006.
49. Finnis KW, Starreveld YP, Parrent AG, Sadikot AF, Peters TM. Three-dimensional database of subcortical electrophysiology for image-guided stereotactic functional neurosurgery. IEEE Trans Med Imaging 2003;22(1):93–104. [PubMed: 12703763]
50. D'Haese PF, Cetinkaya E, Konrad PE, Kao C, Dawant BM. Computer-aided placement of deep brain stimulators: from planning to intraoperative guidance. IEEE Trans Med Imaging 2005;24(11):1469–1478. [PubMed: 16279083]
51. Miocinovic S, Maks CB, Noecker AM, Butson CR, McIntyre CC. Cicerone: Deep brain stimulation neurosurgical navigation software system. Acta Neurochir Suppl 2007;97(2):561–567. [PubMed: 17691348]
52. Butson CR, Noecker AM, Maks CB, McIntyre CC. StimExplorer: Deep brain stimulation parameter selection software system. Acta Neurochir Suppl 2007;97(2):569–574. [PubMed: 17691349]

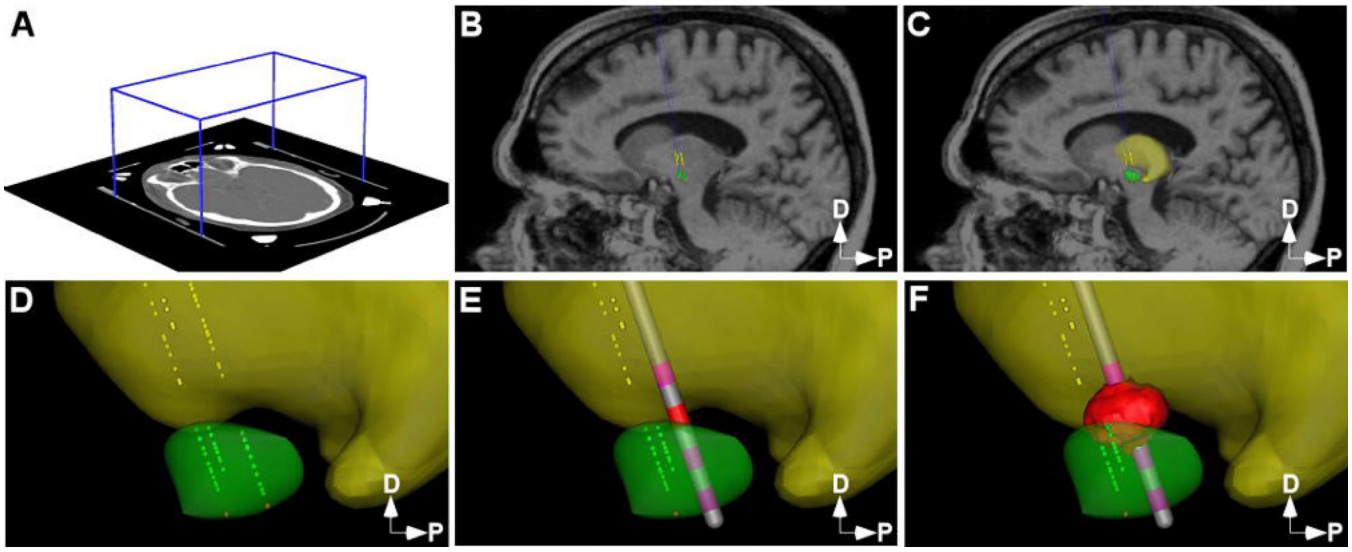

Figure 1.

Patient-specific model of deep brain stimulation. A) Stereotactic coordinate system was defined relative to the imaging data. B) Microelectrode recording data was entered into the model (thalamic cells – yellow dots; subthalamic cells – green dots; substantia nigra cells – red dots). C, D) 3D brain atlas was fit to the neuroanatomy and neurophysiology (yellow volume – thalamus; green volume – subthalamic nucleus). E) DBS electrode was positioned in the model (pink contacts – inactive, red contact – active). F) VTA (red volume) was calculated for the clinically defined therapeutic stimulation parameter settings. D – dorsal, P – posterior. Data presented for Patient 1.

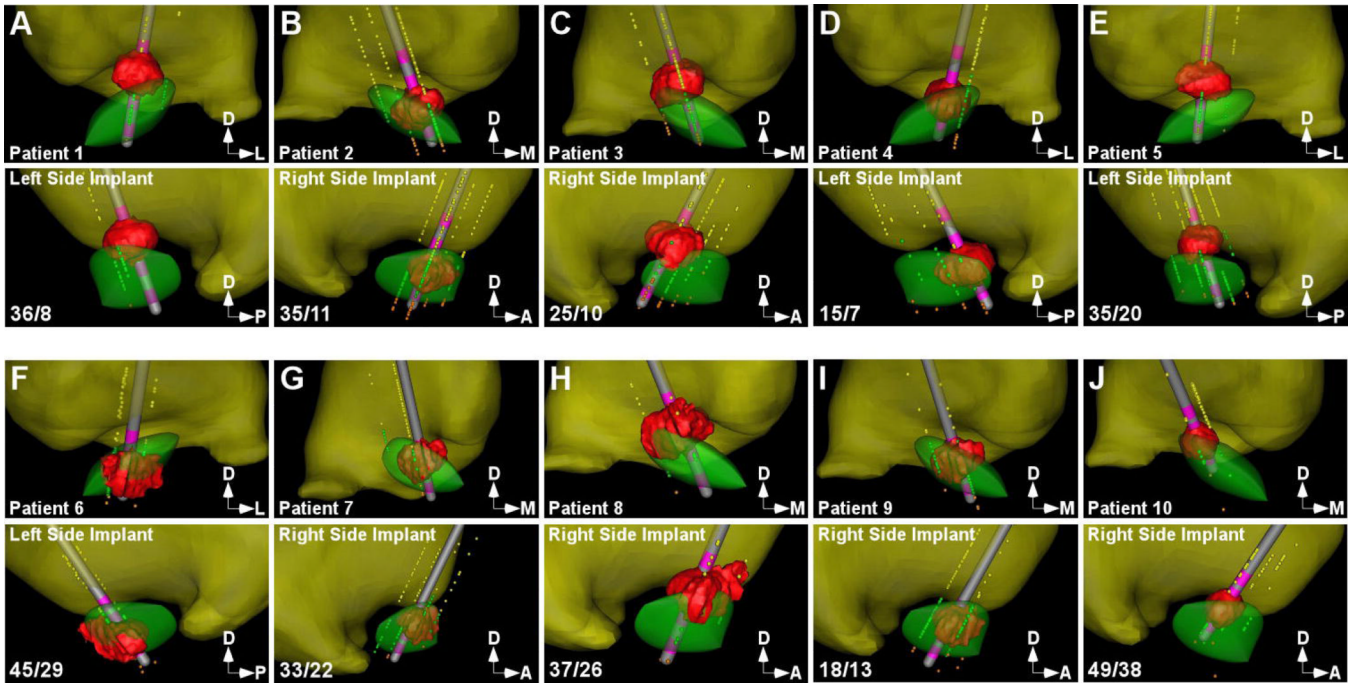

Figure 2.

10 patient-specific models of DBS. Sections A–J correspond to patients 1–10, respectively. Each section consists of two panels. The top panel displays a 3D coronal view, the bottom panel displays a 3D sagittal view. Each panel shows the thalamus (yellow volume), thalamic MER data (yellow dots), subthalamic nucleus (green volume), subthalamic MER data (green dots), substantia nigra MER data (orange dots), DBS electrode, and therapeutic VTA (red volume). The lower left corner of each section lists the OFF MEDS UPDRS motor score in the OFF DBS / ON DBS conditions. D – dorsal, M – medial, L – lateral, A – anterior, P – posterior.

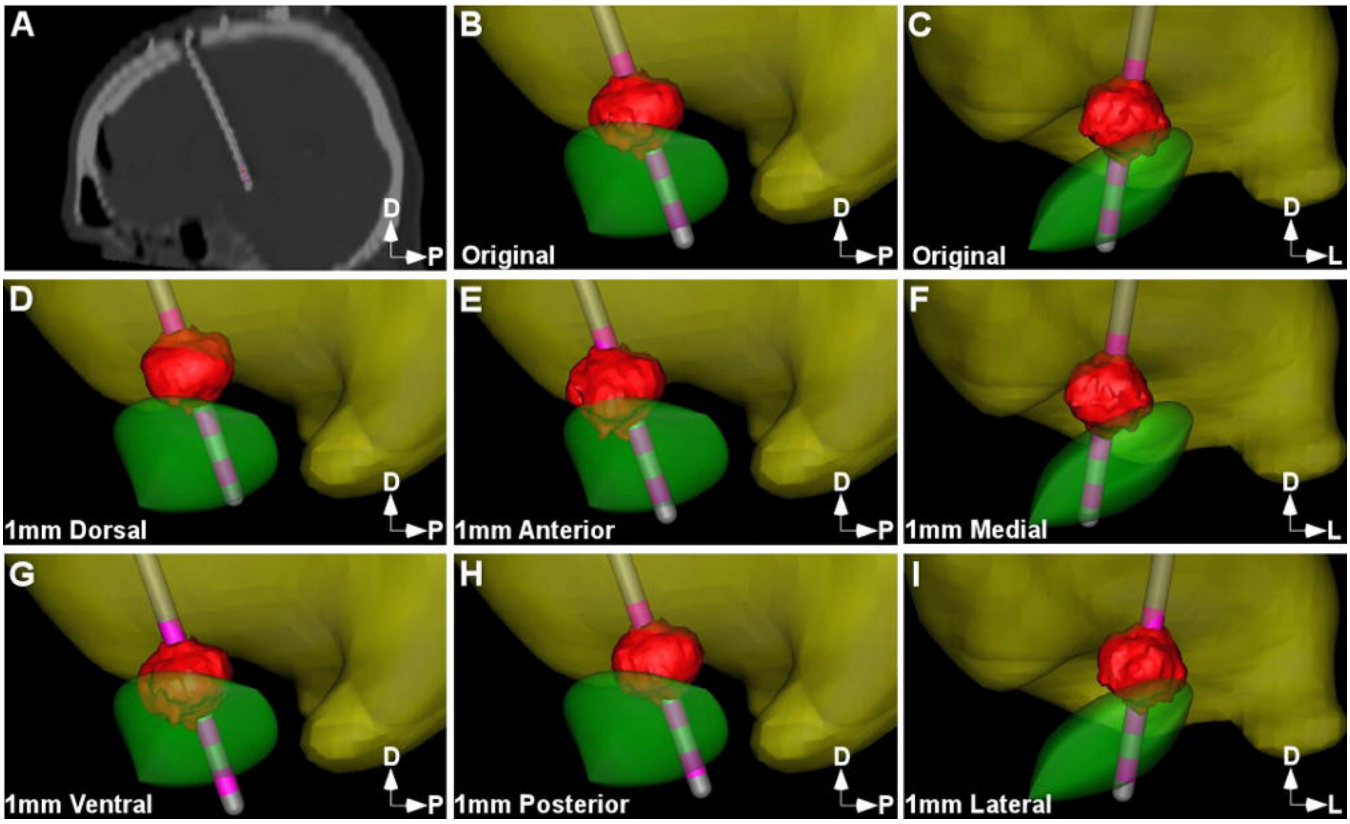

Figure 3.
DBS electrode location sensitivity analysis. A) Post-operative CT (parasagittal slice parallel to the DBS electrode trajectory) depicting the modeled and imaged DBS electrode location. B) 3D sagittal view and C) 3D coronal view of the originally modeled DBS electrode location and VTA. D–I) 1 mm shifts in the DBS electrode location, and for each shifted DBS electrode location the corresponding VTA calculated for the clinically defined therapeutic stimulation parameter settings. Data presented for Patient 1.

Table 1

Clinically Effective DBS Parameters

Patient #	Side	Electrode Model	Contact	Impedance*	Voltage (V)	PW (μs)	Freq (Hz)
1	Left	3387	2	High	−2.3	60	185
2	Right	3387	1	High	−2.3	60	130
3	Right	3387	2	Mid	−3	60	185
4	Left	3387	1	High	−3.5	60	130
5	Left	3387	2	High	−3.6	60	145
6	Left	3389	1	Mid	−2.5	90	185
7	Right	3389	2	High	−2.5	60	130
8	Right	3387	2	High	−3.6	60	185
9	Right	3389	2	High	−2	60	135
10	Right	3389	1	High	−1.5	60	130

*Impedance was accounted for using electrode encapsulation models previously described in Butson et al. [42]. The high impedance model was used if the clinical impedance measured at the specified contact exceeded 1300 Ω and the mid impedance model was used for contacts that ranged between 700 Ω and 1300 Ω.

Table 2

Microelectrode Recording

Patient #	Number of tracks	STN MER points in 3D STN model
1	3	100%
2	6	78%
3	5	75%
4	4	71%
5	4	78%
6	3	100%
7	4	54%
8	3	97%
9	4	83%
10	4	100%

Table 3

Clinical Outcomes

Patient #	Therapeutic VTA (mm^3)	%VTA inside STN	% UPDRS improvement with DBS alone	% UPDRS improvement with MEDS alone
1	51	16%	78%	47%
2	57	78%	69%	69%
3	87	11%	60%	76%
4	65	43%	53%	41%
5	78	5%	43%	40%
6	116	72%	36%	56%
7	69	79%	33%	52%
8	96	35%	30%	41%
9	66	83%	28%	45%
10	30	66%	22%	45%

Table 4

Sensitivity Analysis*

Patient #	VTA (mm^3)	VTA inside STN (mm^3)	VTA outside STN (mm^3)
1	51 ± 3	9 ± 7	42 ± 6
2	58 ± 7	43 ± 12	14 ± 7
3	85 ± 3	10 ± 7	75 ± 7
4	67 ± 2	28 ± 11	39 ± 10
5	78 ± 3	4 ± 4	74 ± 3
6	114 ± 8	77 ± 6	37 ± 13
7	69 ± 10	52 ± 12	17 ± 7
8	96 ± 10	32 ± 11	64 ± 9
9	68 ± 9	50 ± 11	17 ± 6
10	30 ± 1	18 ± 6	12 ± 5

* Average and standard deviation of the activated volume calculated from 7 possible electrode locations given ±1 mm error in electrode localization relative to the anatomy (see Figure 3).